Experiments in Fluids 3, 11–16 (1985)

Experiments in Fluids

Deformation to breaking of deep water gravity waves

P. Bonmarin and **A. Ramamonjiarisoa**

Institut de Mécanique Statistique de la Turbulence, 12, Avenue du Général Leclerc, 13003 Marseille, France

Abstract. The results of laboratory observations of the deformation of deep water gravity waves leading to wave breaking are reported. The specially developed visualization technique which was used is described. A preliminary analysis of the results has led to similar conclusions than recently developed theories. As a main fact, the observed wave breaking appears as the result of, first, a modulational instability which causes the local wave steepness to approach a maximum and, second, a rapidly growing instability leading directly to the breaking.

List of symbols

L	total wave length
H	total wave height
η'	crest elevation above still water level
η''	trough depression below still water level
γ	wave steepness $\gamma = H/L$
γ'	crest steepness $\gamma' = \eta'/L$
γ''	trough steepness $\gamma'' = \eta''/L$
F_1	forward horizontal length from zero-upcross point (A) to wave crest
F_2	backward horizontal length from wave crest to zero-downcross point (B)
ε	crest front steepness $\varepsilon = \eta'/F_1$
δ	crest rear steepness $\delta = \eta'/F_2$
λ	vertical asymmetry factor $= F_2/F_1$ (describing the wave asymmetry with respect to a vertical axis through the wave crest)
μ	horizontal asymmetry factor $= \eta'/H$ (describing the wave asymmetry with respect to a horizontal axis: SWL)
T_0	wavemaker period
L_0	theoretical wave length of a small amplitude sinusoïdal wave generated at T_0^{-1} frequency
$\overline{H_0}$	average wave height

1 Introduction

In recent years, special attention was given to the breaking of gravity waves in deep water because of both fundamental and practical interest. The breaking process constitutes, in principle, the final stage in the development of a wave profile. Until recently, the involved physical mechanism was poorly understood. The situation has been improved since powerful numerical methods have been developed (Longuet-Higgins and Cokelet 1976, 1978; Vinje and Brevig 1980). It has become possible to determine the nature of some of the instability mechanisms leading to the wave breaking.

The breaking itself is responsible for a number of other important physical processes, e.g. the generation of air bubbles, currents, and turbulence in the water body and supposedly the formation of water surface ripples. These phenomena can have a significant influence on the exchange processes at the ocean-atmosphere interface (Merlivat and Memery 1983).

The main objective of our investigation is a better understanding of the physical mechanism of the wave breaking and of some of the aforementioned related processes. The experimental program included the development of a technique for optically recording the deformation of gravity waves generated in a wind-water tank. The observations and measurements led to quantitative values for certain parameters characterizing the deformation of the wave profile. In the following, the experimental procedure will be described, and the first results about the spatial and temporal development of the parameters will be reported and discussed.

2 Facility and experimental procedure

The experiments have been conducted in the IMST (Institut de Mécanique Statistique de la Turbulence) large wind-water tank described in detail by Coantic and Bonmarin (1975). An arrangement, shown schematically in Fig. 1, was used to record, as function of space and time, the deformation of the water surface in the presence of breaking waves. As the movie camera and the lighting device were fixed to a carriage moving at a controlable speed, it was possible to follow the deformation of individual wave crests over a longitudinal distance of several wavelengths.

For visualizing the wave profile, a small quantity of fluorescein was spread over the water surface which was

illuminated by the lighting device shown schematically in Fig. 2. With this arrangement we were able to match a number of requirements prescribed by the cinematographic recording as well as by the physical process to be analyzed. A powerful light source (3×200 Watts) was necessary because of the large distance (~ 1.5 m) between the source and the water surface. The used flash lamps (14 μs flash duration) had a high enough energy level in the ultraviolet range in order to sufficiently excite the fluorescence at the surface. For a well defined recording of the deformation of the wave profile, it appeared highly desirable to illuminate the profile over a longitudinal distance of at least one wavelength. Movies were recorded with a "16 mm Photo Sonic" camera which takes up to 500 frames per second and which was equipped with a lens of 25 mm focal length and an aperture ratio of 0.95 (manufactured by Angenieux). The used colour films Gevachrome 710 and 720 provide images of high contrast and appropriate for subsequent digital processing.

The wavy motion of the water surface was produced by an electro-hydraulic device capable of generating regular as well as random oscillations in the frequency range between 1 Hz and 3 Hz. Preliminary experiments were made with the wave generator oscillating regularly at 1.2, 1.3, 1.4 and 1.5 Hz, with the amplitude being so that the initial wave steepness (in the immediate vicinity of the generator) was of an order of $(H/L)_0 = 0.08$. Recent investigations (Longuet-Higgins and Cokelet 1978; Brondino 1981) show that for such a value of the initial wave steepness, an initially uniform wave train is modulationally unstable, and the instability may lead to breaking. The frequency 1.4 Hz finally was chosen as the basic value in all experiments. Then, the amplitude and the wave length are well adapted to the performance of the visualization equipment described above.

A sample frame from the movie film is shown in Fig. 3. Single frame images of the movie were digitized with a Hewlett-Packard 9874A digitizer. Each wave profile was transformed into a set of X-Y coordinates, and the value numbers (about 500 per wavelength) stored in a Hewlett-Packard 85 minicomputer for further processing.

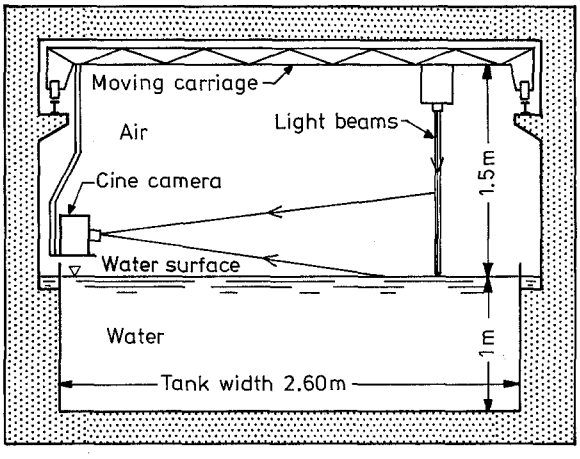

Fig. 1. Overall schematic view of visualization system

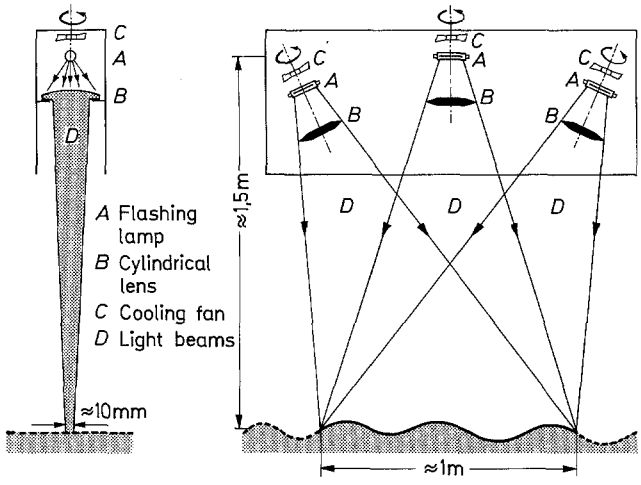

Fig. 2. Schematic diagram of the lighting device

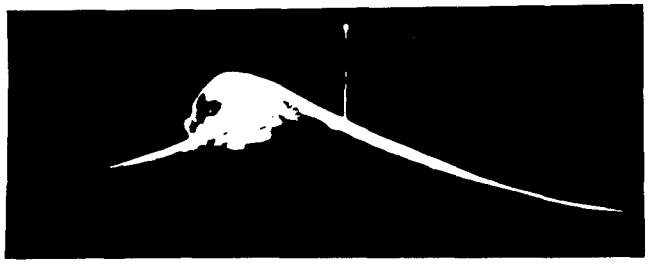

Fig. 3. Photograph of a plunging breaker observed in the water tank (from a 16 mm movie film)

3 Results

Figure 4 shows a typical example of the crest deformation for a plunging breaker together with the deformation predicted by the numerical study of Vinje and Brevig (1980). The qualitative similarity between the observed and the calculated deformation is obvious.

The initial wave steepness $(H/L)_0$ during the present experiments was of the order of 0.08. The analytical investigation of Longuet-Higgins and Cokelet (1978) predicted that for such a steepness value the wave train would first suffer a modulational instability of the Benjamin-Feir type. Later on, the local wave steepness may reach values close to the maximum of 0.14 and develops a fast-growing instability leading directly to the breaking. A previous experimental study (Brondino 1981) showed quite clearly the existence of the two successive instabilities. Furthermore, quantitative agreement was found between the analytical and the experimental results which concern the development of the modulational instability.

The present work is mainly concerned with the instability of the second type, which is responsible for the wave breaking. Unlike the case of the modulational instability, a detailed comparison between the analytical and the experimental results is difficult to handle here because, in particular, the local scales of length and time which characterize the instability are not sufficiently known, neither analytically nor experimentally. Longuet-Higgins and Cokelet (1976) found the final stages of the breaking waves to be very similar in all cases (various initial wave steepness) they considered. This appears to be confirmed by comparing their analytical results (Longuet-Higgins and Cokelet 1978) with the results of the present experiments, as shown in Fig. 5. In the analysis, the instability is due to the effect of a pressure field above the water surface, applied during a small fraction of the wave period, whereas we observed in the experiments that the instability develops, after a critical value of the local wave steepness was reached through a subharmonic instability. Nevertheless, the final stages of the wave breaking are qualitatively very similar in both cases. In the analysis the duration of this stage, as expected, was found to depend upon the pressure amplitude. From the experiments where the waves are free from the action of an external pressure, this duration is found to be of the order of 30% of the basic wave period. The breaking constitutes a strong nonlinear process. Taking into account that there exist significant differences between our observations and the assumptions made for the numerical calculations by the authors cited above, no detailed comparison between the two types of results was attempted. However, such a comparison obviously is necessary and will constitute one of the main aims of our future work which will include the two types of approaches referred to above.

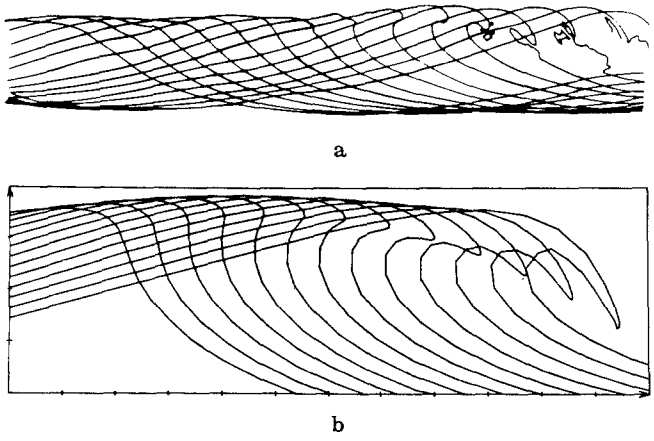

Fig. 4a and b. Comparison of observed (**a**) and computed (**b**) crest chronological evolution; **a** time between two successive frames $\simeq$ 0.04 s; **b** numerical study by Vinje and Brevig (1980)

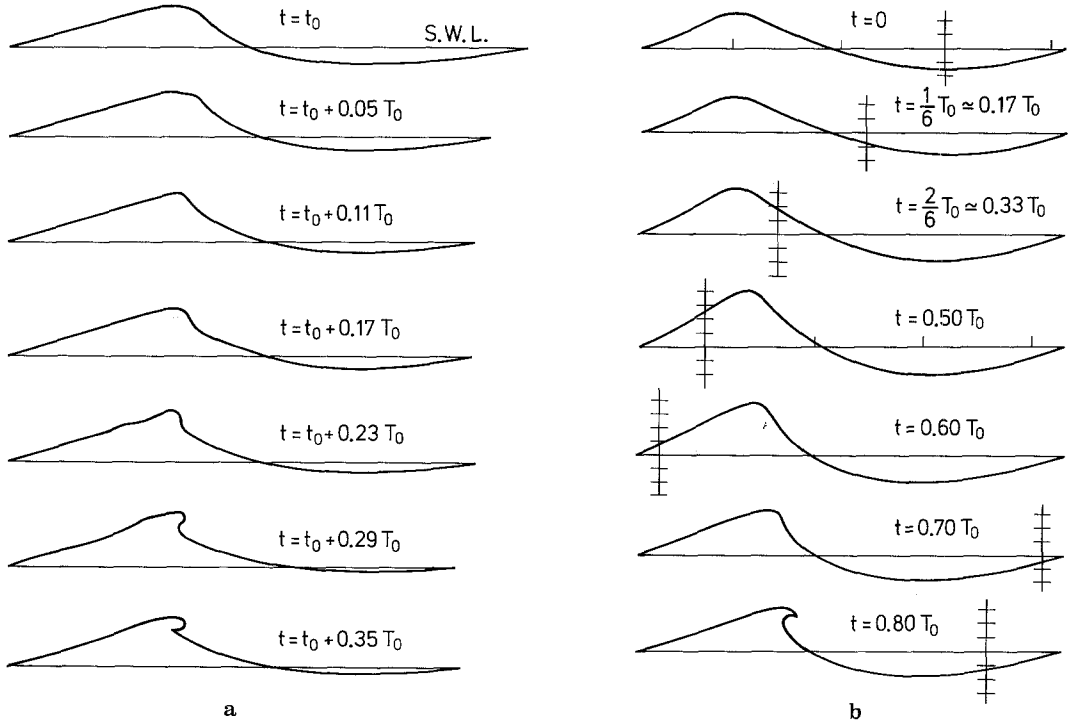

Fig. 5a and b. Comparison of observed (**a**) and computed (**b**) breaking wave profiles; **a** from a 16 mm cine-film 24 f/s; **b** from Longuet-Higgins and Cokelet (1975)

The deformation of the wave profile was described in terms of the geometrical parameters defined in Fig. 6 and listed in the list of symbols. In this, we follow a suggestion by Kjeldsen and Myrhaug (1978) for characterizing a wave profile when it deviates from a symmetrical waveform (both in vertical and in horizontal direction). The experimental procedure we have used appeared particularly appropriate to accurately define, as function of space and time, the development of these parameters during the rapid deformation of the profile. It is of interest to note that the horizontal and vertical scales of the wave are referred to the water surface level at rest and not to the mean surface level, as it was done in most of the numerical investigations.

To each frame in a sequence of data, e.g. that shown in Fig. 4, corresponds a set of parameters obtained after digitizing the date and using a simple program for calculating the parameters. In the following the results showing their development are presented and briefly discussed.

Figure 7 shows the variation of the wavelength of an individual wave during a period of time which includes the breaking event. It is seen that the wavelength decreases monotonically before and even after the breaking. This appears to be in agreement with the numerical result of Longuet-Higgins and Cokelet (1978) who showed that, for a wavetrain with an initial wave steepness H/L less than 0.09, the decrease in wavelength is necessary for the individual wave to reach the point of breaking. Indeed, the

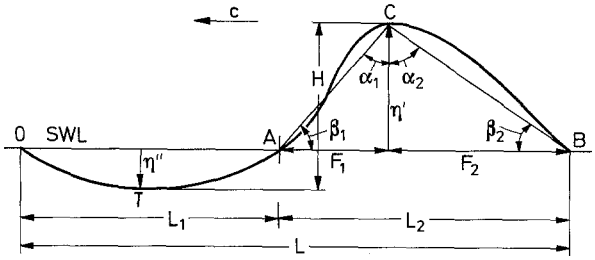

Fig. 6. Definition of wave parameters

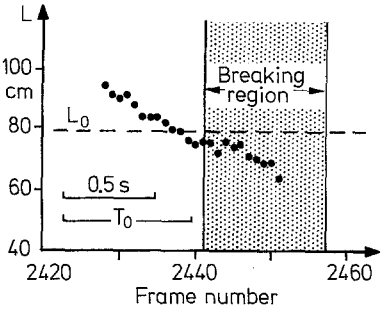

Fig. 7. Total wavelength versus cine-film frame number (inter-frame time $\simeq$ 0.04 s)

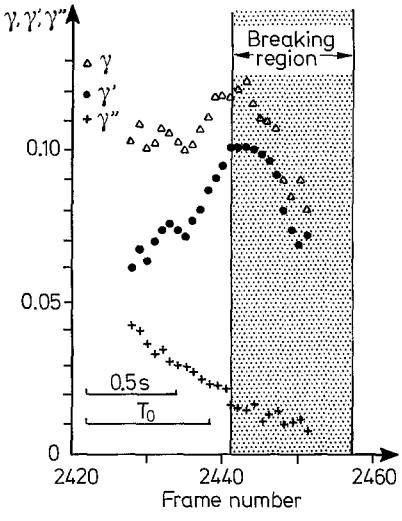

Fig. 9. Wave steepness, crest and trough steepness versus cine-film frame number (inter-frame time $\simeq$ 0.04 s)

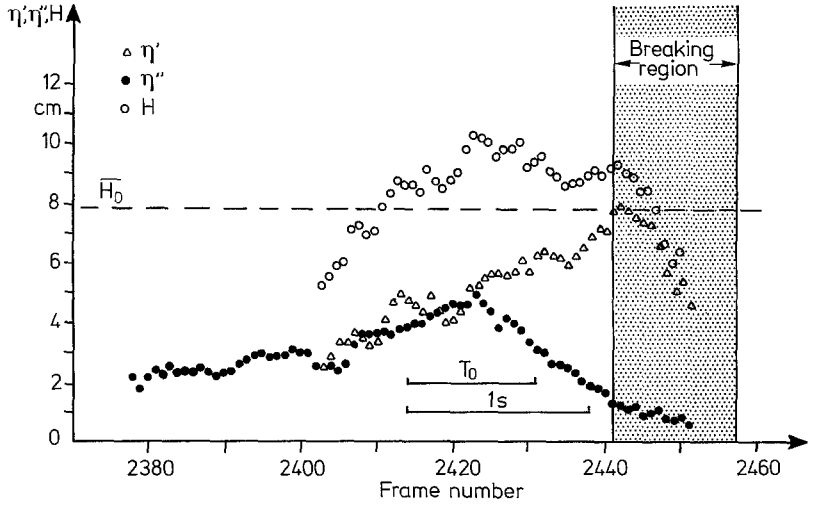

Fig. 8. Total wave amplitude, crest elevation and trough depression, versus cine-film frame number (inter-frame time $\simeq$ 0.04 s)

latter would be the result of the combination of an increase of the wave amplitude together with a decrease of the wavelength. In such a way, a maximum of the wave steepness may be obtained locally.

Such a conclusion is confirmed by our observations of the wave height and the development of the wave steepness, as shown in Figs. 8 and 9, respectively. The wave height first increases and then slowly decreases. After the breaking point, the wave height decreases very rapidly, as expected. The development of the wave height obviously is the consequence of the relative variation of the crest elevation and the trough depth. First, both variables simultaneously increase leading to the monotonic increase of the wave height. But, while the crest elevation continues to increase until the breaking point is reached, the trough depth rapidly decreases. As a consequence the wave height has a tendency to slowly decrease. Once the breaking has occurred, the crest elevation decreases rapidly while the trough depth tends to become zero. The latter observation could be of interest for a better understanding of the wave profile instability. It follows that there is a concentration of water mass above the water surface level at rest.

Of special interest is the development of the individual wave steepness as shown in Fig. 9. The variation of the combination of wavelength and wave height results in a net increase of the wave steepness up to a maximum of about 0.12 at the breaking point. This value agrees with the numerical prediction of Longuet-Higgins and Cokelet (1978). It is seen that the "crest steepness" increases even more rapidly than the wave steepness, while the "trough steepness" decreases rapidly to a value close to zero. This result again confirms the observed tendency of the water mass to be concentrated above the water surface level at rest. This result also was expressed in terms of the variation of the horizontal asymmetry factor μ. It was found that this factor increases rapidly from a value of about 0.5, which corresponds to a symmetrical waveform, to a value of about 0.85 at the breaking point. For different types of breaking waves, Kjeldsen and Myrhaug (1979) found an horizontal asymmetry factor in the range from 0.84 to 0.95, with the highest values for the plunging breakers.

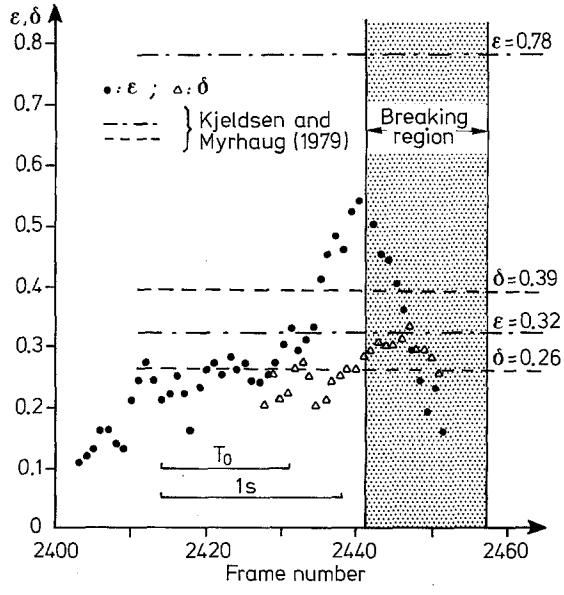

Fig. 10. Crest front steepness and crest rear steepness versus cine-film frame number (inter-frame time $\simeq$ 0.04 s)

Figure 10 shows the variation of the crest front steepness ε and the crest rear steepness δ. At the beginning both factors have a value of about 0.25. But, while δ experiences only a slight variations, ε increases rapidly up to a value of about 0.55 which is reached at the breaking point. This rapid variation appears to be the result of the rapid increase of the crest elevation η' (see Fig. 8) together with a rapid decrease of the "forward length" F_1. Our hope was to find for these parameters some "universal" values at the breaking point in order to define a criterium for the wave breaking. It appears that such values do not exist. The observed values apparently are in the ranges previously defined by Kjeldsen and Myrhaug (1979), namely between 0.26 and 0.39 for δ and between 0.32 and 0.78 for ε. Further detailed studies related to these factors are in progress.

4 Conclusions

A technique for visualizing the profile of deep water gravity waves in a wind wave tank has been described. The technique was used to measure the variation in space and time of a number of parameters which characterize the wave profile. The measurements were performed during the period of the fast growing instability leading to the wave breaking. A preliminary comparison between the observations and the results of recent analytical studies led to fair quantitative agreement. Particularly, in agreement with the results of Longuet-Higgins and Cokelet (1978) it was found that the breaking is due to the combined effect of a rapid increase of the local wave height together with a rapid decrease of the wavelength. As a consequence, the local wave steepness has a value of about 0.12 which is compatible with the observed breaking. During a period of time of the order of the wave period, the other factors which characterize the wave profile were found to vary rapidly before the breaking point was reached.

Acknowledgements

We gratefully acknowledge financial support provided by the Centre National pour l'Exploitation des Océans (C.N.E.X.O.) under Grant N° 81/2551 and N° 83/2840 and the Centre National de la Recherche Scientifique (C.N.R.S.). We also thank to the Photographic and Cinematographic Laboratory in the Centre d'Essais de la Méditerranée (C.E.M.) for its valuable technical help.

References

Brondino, G. 1981: Contribution à l'étude de la stabilité des ondes de gravité. Thesis, Univers. of Aix-Marseille II

Coantic, M.; Bonmarin, P. 1975: The air-sea interaction simulation facility at the Institut de Mécanique Statistique de la Turbulence. Atmospheric Technology 7, 72–79

Kjeldsen, S. P.; Myrhaug, D. 1978: Kinematic and dynamics of breaking waves. Report n° STF 60 A 78200, Ships in Rough Seas, Part 4, Norvegian Hydrodynamic Laboratory, Trondheim

Kjeldsen, S. P., Myrhaug, D. 1979: Breaking waves in deep water and resulting wave forces. 11th Annual OTC in Houston no. 3646

Longuet-Higgins, M. S.; Cokelet, E. D. 1976: The deformation of steep surface waves on water. I – A numerical method of computation. Proc. Roy. Soc. Lond. A 350, 1–26

Longuet-Higgins, M. S.; Cokelet, E. D. 1978: The deformation of steep surface waves on water. II – Growth of normal-mode instabilities. Proc. Roy. Soc. Lond. A 364, 1–28

Merlivat, L.; Memery, L. 1983: Gas exchange across an air-water interface: Experimental results and modeling of bubble contribution to transfer. J. Geophys. Res. 88, 707–724

Vinje, T.; Brevig, P. 1980: Breaking wave on finite water depths. A numerical study. Rep. Norvegian Hydrodynamic Laboratory, Trondheim

Received May 5, 1984